Proceedings of ERAD (2002): 227–232 © Copernicus GmbH 2002

ERAD 2002

# Reconstruction of rainrate fields in complex orography from C-band radar volume data

**F. S. Marzano**[1], **E. Picciotti**[2], **and G. Vulpiani**[1]

[1]Centro di Eccellenza CETEMPS Dipartimento di Ingegneria Elettrica e Dipartimento di Fisica, Università dell'Aquila Monteluco di Roio, 67040 L'Aquila, Italy
[2]Parco Scientifico e Tecnologico d'Abruzzo Via Antica Arischia, 1 – 67100 L'Aquila, Italy

**Abstract.** A hybrid technique to reconstruct near-surface rainrate fields from high-elevation reflectivity bins in presence of a complex orography is proposed. The method is based on the statistical analysis of a large reflectivity volume data set, classified into stratiform and convective rain regimes and re-sampled onto a uniform Cartesian grid by means of an adaptive Cressman approach. Principal component decomposition is applied to the data set in order to extract significant reflectivity-profile variance. A retrieval technique, based on a non-linear statistical scheme, is then used to infer near-surface reflectivity from available high-altitude echoes at a given range interval. Finally, a three-layer neural network technique is set up in order to estimate surface rainrate from reconstructed near- surface reflectivity fields. The proposed hybrid technique is illustrated by using volume data acquired by the C-band Doppler radar, operated in L'Aquila (Italy). A case study, related to a rainfall event that occurred in L'Aquila region during fall 2000, is discussed.

## 1 Introduction

The reconstruction of rainrate fields represents a valuable information not only for radio-propagation channel planning and hydro-geological applications, but also for assimilation purposes within numerical weather forecast models. In presence of a complex orography characterized by hilly and mountainous scenarios, this task is fairly involved especially if needed at a ground resolution less than few kilometers (Joss and Lee, 1995; Andrieu and Creutin, 1995; Vignal et al.,2000). Rain gauge networks denote many limitations related to their sparse and spot-like data distribution. Nevertheless, they represent indispensable means for remote-sensor calibration and validation (Ciach and Krajewski, 1999).

Microwave Doppler radars are considered a fairly established technique to retrieve rainrate fields from measured reflectivity volumes (e.g., Sauvageot, 1992; Marzano et al 1994; Borga et al.,2000). However, in a complex orographic environment radar observations are affected by several impairments which should be carefully evaluated. Together with the enhancement of ground-clutter effects, the major limitation is represented by partial or total beam blocking caused by natural obstructions which very often impose scanning elevations higher than 1.5° (Joss and Lee, 1995). These range-related limitations tend to reduce the potential role of operational weather radars in monitoring precipitation amount at ground within mountainous areas since, if either the nature or intensity of rainfall varies with height (e.g., melting effects during stratiform rain), radar returns at higher altitudes may be not representative of surface rainrate (Andrieu and Creutin, 1995; Ciach and Krajewski, 1999; Gray et al., 2002) In this work, we propose a hybrid technique to reconstruct near-surface reflectivity fields from high-elevation reflectivity bins in presence of highly variable orographic obstructions. A combined principal component decomposition and a non-linear multiple regression scheme is used to infer near-surface reflectivity from available high-altitude echoes at a given range interval. A three-layer neural network technique is set up in order to estimate surface rainrate from reconstructed near-surface reflectivity fields. To mitigate mean-field bias due to the rain gauge point measurements, rain gauge data are spatially interpolated by means of a statistical method to produce a surface rainfall field compatible with areal radar estimates. A case study, related to rainfall events observed by a C-band Doppler radar operated in L'Aquila (Italy), is illustrated.

## 2 Radar remote sensing in complex orography

Radar rainfall retrievals are, as said, affected by several ambiguities which need to be carefully corrected and, possibly, removed before any attempt to use radar estimates in an operational context (Joss and Lee, 1995). In a complex orography, surface rainfall might be even not observed at all for a large portion of the radar volume scan. Besides practical

*Correspondence to:* F. S. Marzano (marzano@ing.univaq.it)

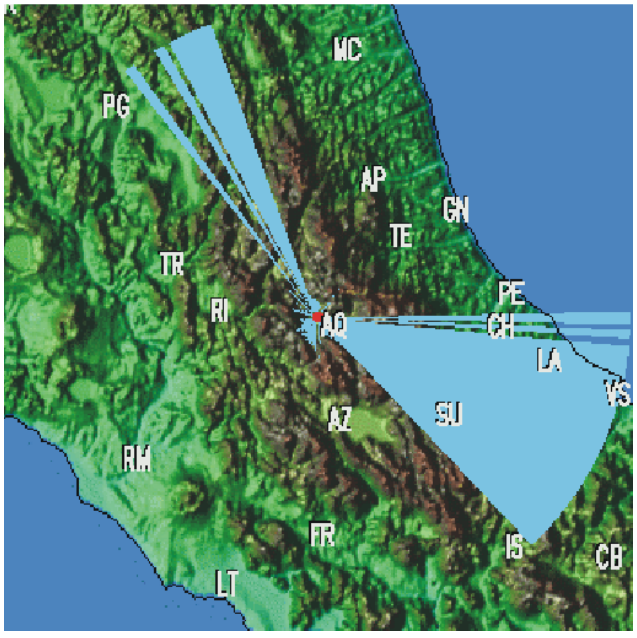


**Fig. 1.** Radar visibility map at 2° elevation, relative to the Abruzzo radar placed in L'Aquila (Italy).

and legal problems, the choice of a radar site operating in complex orography is a cumbersome task. On one hand, the goal is to select it as high as possible in order to increase radar coverage, but on the other hand the higher is the site the more complicate becomes the impact of mixed-phase rainfall (around the freezing level) and the extrapolation of estimates to ground level.

### 2.1 C-Band Doppler radar

Volume data, gathered by a C-band Doppler Abruzzo radar placed in L'Aquila (Italy) at 680-m altitude, will be used in this work. The single-parameter radar is placed on a 10-m height tower at 42.38° latitude and 13.32° longitude, having a radome-covered parabolic antenna of 2.44-m diameter, a 1.6° half-power beamwidth and 40-dB directivity. The magnetron peak-power is 250 kW at 5.6 GHz with a pulse repetition frequency (PRF) of 250 Hz (i.e., *intensity* mode with a pulse width of 1.98 $\mu$s) and 787, 885 and 1180 Hz (i.e., *velocity* mode with unfolding option and a pulse width of 0.75 $\mu$s). The receiver sensitivity is equal to $-110$ dBm. The maximum range is 480 km and 120 km for the intensity and velocity mode, respectively. A self-contained software, named EDGE by EEC Inc., is used to remotely operate and archive radar data.

Figure 1 shows the visibility map at 2° elevation superimposed to a digital elevation model of Central Italy around L'Aquila (AQ symbol), located in the middle of Apennine mountain range extending along the length of the Italian peninsula. Eastward the Gran-Sasso mountain (with peaks up 3000 m) clearly blocks radar beams.

Almost the same happens westward due to the Velino and

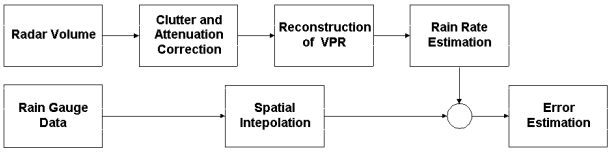


**Fig. 2.** Block diagram of the radar rainfall retrieval algorithm, adopted for the Abruzzo radar.

Sirente mountains. As evident, the orography is such that the radar visibility at low elevations is ensured only in the south-east directions within a sector of about 45°. This radar location was, indeed, chosen to monitor the Aterno river valley, going from L'Aquila to Sulmona (SU symbol) along the South-East direction.

### 2.2 Rainfall retrieval algorithm

A radar rainfall retrieval in complex orography should basically try to solve the problem of beam blockage in order to provide a useful hydro-meteorological product. However, all the classical steps of radar data processing must be carefully carried out.

The general radar equation expresses the received power $P_R(r,\theta,\phi)$ from a volume at range $r$ along elevation-azimuth directions $(\theta,\varphi)$ as shown by Sauvageot (1992):

$$P_R(r,\theta,\varphi) = C\frac{Z_a(r,\theta,\varphi)}{r^2}e^{-2A(r,\theta,\varphi)}\,, \qquad (1)$$

where $C$ is the instrumental constant, $Z_a$ the apparent reflectivity [mm$^6$ m$^{-3}$] and $A$ the one-way path attenuation. It is worth mentioning that the apparent reflectivity $Z_a$ is equal to the equivalent reflectivity $Z$ of an observed radar volume only if non-uniform beam filling of the volume itself is negligible (Andrieu and Creutin, 1995). The latter condition might be not true at longer ranges ($>$ 60 km) (Vignal et al., 2000). However, in this work we will assume that $Z_a = Z$ at any range.

Figure 2 illustrates the block diagram of the overall retrieval algorithm. De-cluttering is of particular importance in complex orography. We have adopted the scheme proposed by Joss and Lee (1995), based on the construction of an areal clutter map. The latter is obtained by averaging, for each range gate, the volume reflectivity measurement in clear-air conditions at least every month. However, the scheme has been integrated with spectral and statistical signal processing, routinely performed by EDGE using signal temporal autocorrelation, histogram and Doppler velocity analysis.

Classification of rain events into stratiform and convective regimes is carried out by using a reflectivity horizontal gradient and intensity technique (Steiner et al., 1995). Significant path attenuation $A(r,\theta,\varphi)$, due to convective rainfall, is corrected by using an iterative forward algorithm (Aydin et al., 1989; Marzano et al., 1994). The reconstruction of the vertical profiles of reflectivity (VPR) is one of the principal steps when operating in a complex environment. If $\mathbf{u} = (x,y)$ is

the geographical location and $h$ is the altitude, normalized VPR is defined as follows:

$$z(h) = \frac{Z(r,\theta,\varphi)}{Z_o(r,\theta,\varphi)} = \frac{Z(\mathbf{u},h)}{Z(\mathbf{u},h=0)} \quad (2)$$

where $Z_o$ is a reference reflectivity at ground level. Generally, $z(h)$ is assumed to be the same at any point $\mathbf{u}$ of the studied area and independent of the rainfall horizontal variability (at least in a sub-region). Most attempts tend to tackle with (2) by using inverse techniques (see next paragraphs).

Once reconstructed, near-surface bins of VPR can be used to derived surface rainfall rate (R). A comparison with raingauge-measured rainrate can give a measure of the radar error retrieval, even though major discrepancies can arise from the comparison between an radar areal estimate and a gauge point measurement (Borga et al., 2000; Ciach and Krajewski, 1999).

This problem, sometimes called "mean rainrate-field bias", can be partially reduced by spatially interpolating raingauge measurements (see next paragraph).

## 3 Case study of 7 November 2000

A case study, related to a rainfall event occurred in Abruzzo region during fall 2000, is described and used to illustrate in detail the retrieval technique. The basic steps are similar to those described in literature (e.g., Joss and Lee,1995; Delrieu et al., 2000; Gray et al., 2002).

### 3.1 Radar volume data

Figure 3 shows a Plan Position Indicator (PPI) map acquired on 7 November 2000 by the C-band radar at a range resolution of 250 m after de-cluttering. A continuous acquisition was carried out between 08:00 UTC and 24:00 UTC. Using a $0.5^\circ \times 1^\circ$ azimuth-elevation angular resolution and limiting elevation to $7^\circ$, a single radar volume was completed in about 8 minutes. A total of 48 radar volumes were available for this stratiform event. Note that for convective rain the time interval between two successive volume scans is usually decreased from 20 to 10 minutes.

The measured PPI shows an increase of reflectivity in the South-East directions, denoting a moderate precipitation going on. The rain event lasted about 15 hours, slightly dissipating around 12:00 UTC and re-enhancing from 17:00 UTC until 23:00 UTC.

### 3.2 Rain-gauge network data

Raingauge data from a regional network were available in correspondence of the rainfall event. The network of 40 tipping-bucket rain gauges is sparse and unevenly distributed due to the mountainous geographical conformation.

In order to mitigate the mentioned mean rainrate-field bias, we have applied the modified Cressman (1959) spatial interpolation technique to available raingauge data, hourly sampled. The regular square grid, having 1-km step and 240-km

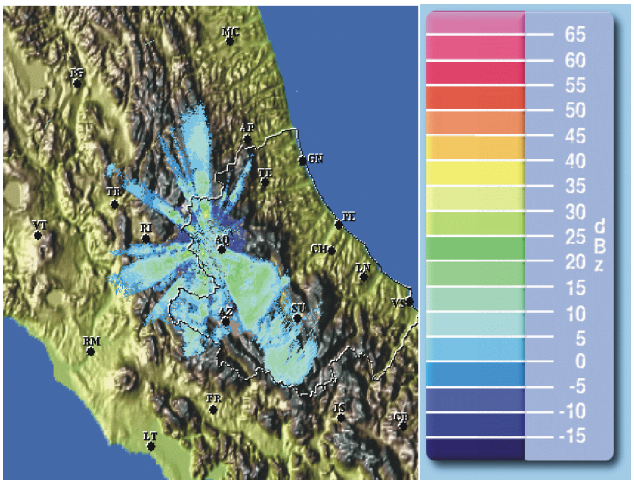


**Fig. 3.** PPI map at $4^\circ$ elevation acquired at 09:00 UTC on 7 November 2000.

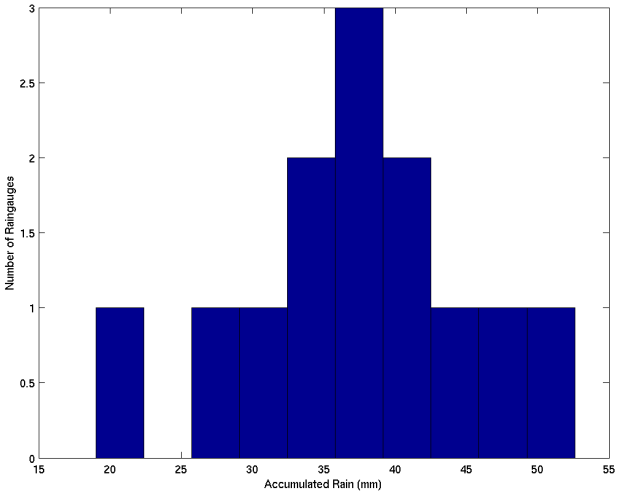


**Fig. 4.** Histogram of the daily accumulated rainfall derived from the rain-gauge network on 7 November 2000.

width, has been centered on the radar site. The influence of contiguous measurements on a given point is defined by an appropriate weighting function whose shape is, in general, elliptic. The latter choice gives the flexibility to allocate the influence shape as a function of local orography. A spatial filter is finally applied to smooth local irregularities. The modified Cressman technique yields rain fields similar to those obtainable from a classical Krige technique, ones the influence radius is set up equal to the Gaussian spatial standard deviation.

As an example referred to this case study, Fig. 4 shows the histogram of the daily accumulated rainfall, using all the available rain gauges during the event (only data larger than 10 mm are plotted). An average of 40-50 mm were accumulated during the day of 7 November 2000.

## 4 Reconstruction of reflectivity vertical profiles

Different techniques to reconstruct near-surface reflectivity fields from high-elevation reflectivity bins in presence of an orographic obstruction are here illustrated. The statistical methods are trained by large reflectivity volume data sets, classified in terms of rainfall typology (e.g., stratiform and convective). The radar volumes are resampled onto a uniform Cartesian grid with 1-km horizontal resolution (covering an area of $240 \times 240$ km$^2$) and 0.5 km vertical resolution (up to 4 km above ground level, i.e. 8 levels). Notice that, due to the inherent spatial degradation of radar bins, the number of available bins decreases as range increases. A Cressman interpolation technique in the horizontal plane with an influence radius of 1 km has been adopted to uniformly fill the 3-D grid.

Three reconstruction approaches have been considered using, as a training data set, resampled radar measurements of moderate stratiform events, acquired during the spring 2000 at ranges less than 40 km in the South-East directions. After training, the reconstruction technique are applied to areas where the beam blocking affects the radar measurements.

### 4.1 Areal average reconstruction (AAR)

A simple technique, consisting in choosing an areal average reflectivity as a reconstructed profile, is considered as a reference (Andrieu and Creutin, 1995; Vignal et al., 2000). Usual approaches to reflectivity profile reconstruction are based on this method. In this case, the normalized VPR is given by:

$$z(h) \cong \langle z(h) \rangle = \frac{\langle Z(|\mathbf{u}|, h) \rangle}{\langle Z_o(|\mathbf{u}|) \rangle} \tag{3}$$

where the angle brackets indicate time-space ensemble averaging of $Z$ profiles, available within the training set, at a given height $h$ at any distance $|\mathbf{u}|$.

### 4.2 Statistical non-linear reconstruction (SNR)

A decomposition of VPR vector $\boldsymbol{z}$ into empirical orthogonal functions is first carried out by (Marzano et al., 1994):

$$\boldsymbol{z} = [z(hj)]_{j=1,N} = \sum_{i=1}^{N} c_i \boldsymbol{z}_i \tag{4}$$

where $N$ is the number of altitude levels of the volume grid (here, $N = 8$), $c_i$ are the principal components and $\boldsymbol{z}_i$ the normalized VPR orthogonal empirical function or eigenvectors. Variance analysis reveals that only the first $M < N$ principal components are necessary to explain more than 90% data variance (in this work, $M = 3$). Then, a multiple quadratic regression can be applied to estimate the $M$ principal components, i.e. here $c_1$, $c_2$ and $c_3$ using available VRP at higher levels:

$$\hat{c} \equiv [c_i]_{i=1,M} = a_o + \sum_{k=1}^{2} \sum_{j=N_o}^{N_M} a_j \Big[ z(h_j) \Big]^k \tag{5}$$

where $a_j$ are the regression coefficients, while $N_o$ and $N_m$ are the lowest and highest levels of available reflectivities at distance $|\mathbf{u}|$ (here, $N_o = 3$ and $N_m > 5$).

### 4.3 Neural network reconstruction (NNR)

A 3-layer neural network (French et al., 1992) with a back-propagation learning method has been implemented with $K_i = N - N_o + 1$ input nodes (here, $K_i = 6$) and $K_o = N_o - 1$ output nodes (here, $K_o = 2$). A sigmoid activation function has been chosen with $K_i/2$ inner nodes. A functional relation between inputs and outputs can be written as:

$$[z(h_j)]_{j=1,K_o} = NN\Big( [z(h_j)]_{j=N_o,N} \Big) \tag{6}$$

where $NN$ is the neural-network functional.

Each network layer is made up of several nodes, and layers are interconnected by sets of correlations weights. The nodes receive input from either outside the initial inputs or from the interconnections. Nodes operate on the input transforming it to produce an analogue output called the firing rate. The weights function to multiply an incoming firing rate prior to its arrival at the next rate. The transformation associated with each node is a sigmoid function defined as

$$f(x) = \frac{1}{1 + \exp(-\beta(x - \theta))} \tag{7}$$

where $x$ is the input to the node, $f(x)$ is the node output or firing rate, $\beta$ is the gain, and $\theta$ is the bias. The values $\beta$ and $\theta$ may either be specified to be: (1) the same for the entire $NN$; (2) different for each layer; or (3) different for each node in the layer. In the $NN$ developed here the first method is utilized.

### 4.4 Tests and inter-comparison analysis

The three reconstruction techniques have been tested on the same case-study data using radar bins within 60-km range. Note that, $Z$ values at surface have been extrapolated from $Z$ at 500 m above ground level. Results are shown in Fig. 5 in terms of mean and standard deviation of the error profile for altitudes less than 2 km.

The better accuracy of SNR and NNR against AAR is apparent, with a slight predominance of SNR performances with respect to NNR. Analogous results have been obtained considering other stratiform and convective cases.

## 5 Estimate of near-surface rainrate

Once reconstructed the entire profile of reflectivity at any position $\mathbf{u}$, surface rainrate can be retrieved by using the near-surface $Z$ through:

– a ZR climatological relationship, as the Marshall-Palmer one (Sauvageot, 1992) or the one proposed by Joss and Lee (1995);

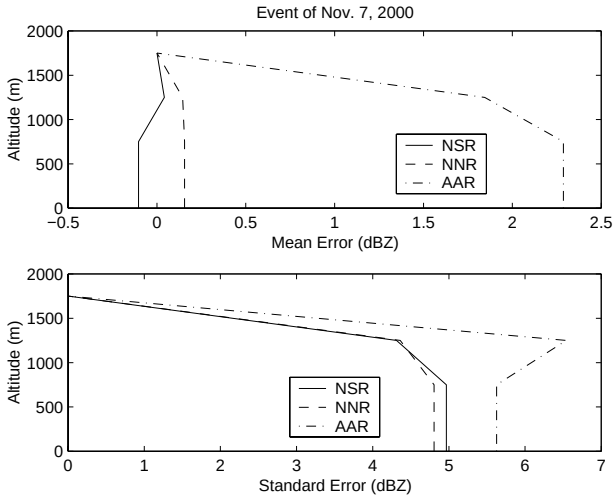


**Fig. 5.** Error mean (top) and standard deviation (bottom) profile, due to VRP reconstructions applied to the test set.

– a neural-network (NN) method, similar to that expressed in (6), but referred to with 3 and 1 nodes at input and output layers, respectively.

The spatially-interpolated raingauge field enables a comparison with radar estimates even at grid points where rain gauges are not present.

In order to evaluate the results, radar-estimated rainrates will be compared with raingage-measured $R$ by using a set of error indicators. If the rainrate retrieval error is expressed as:

$$\varepsilon_R = \hat{R} - R \tag{8}$$

and if the angle brackets indicate the ensemble averaging over available rain gauges and time steps, we can introduce the following error parameters:
- the Fractional Mean Reduction (FMR), defined as

$$FMR = \frac{\langle R \rangle - \langle \varepsilon_R \rangle}{\langle R \rangle} \tag{9}$$

whose optimal value is 1;
- the Fractional Variance Reduction (FVR), defined as:

$$FVR = \frac{\sigma_R^2 - \sigma_{\varepsilon_R}^2}{\sigma_R^2} \tag{10}$$

whose optimal value is 1 and where $sigma^2$ stands for variance;
- the Fractional Standard Error (FSE), defined as:

$$FSE = \frac{\sqrt{\langle \varepsilon_R^2 \rangle}}{\langle R \rangle} \tag{11}$$

whose optimal value is 0;
- the Mean-field Ratio Bias (MRB), defined as:

$$MRB = \left\langle \frac{\hat{R}}{R} \right\rangle \tag{12}$$

whose optimal value is 1.

**Table 1.** Radar-raingauge error indicators, obtained by applying ZR (top) and NN (bottom) methods and two VPR reconstruction techniques to radar data on 7 November 2000.

| Errors using ZR relationship | | | |
|---|---|---|---|
| | VPR by NNR | VPR by SNR | No VPR |
| FMR | 1.76 | 1.72 | 1.64 |
| FVR | 0.04 | 0.04 | -0.05 |
| MRB | 0.24 | 0.29 | 0.36 |
| FSE | 0.51 | 0.47 | 0.48 |
| **Errors using NN techniques** | | | |
| | VPR by NNR | VPR by SNR | No VPR |
| FMR | 0.87 | 0.91 | 0.38 |
| FVR | 0.58 | 0.62 | -0.37 |
| MRB | 1.09 | 1.07 | 1.49 |
| FSE | 0.33 | 0.27 | 1.94 |

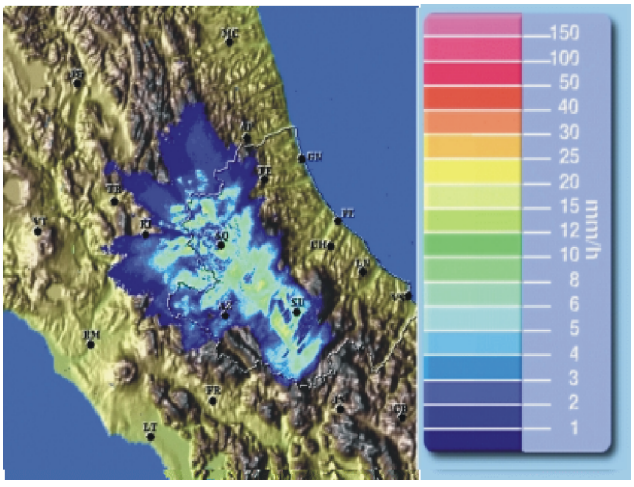


**Fig. 6.** Rainrate retrieved by NN at 09:00 UTC on 7 November 2000.

Table 1 show the results for $ZR$ and $NN$ techniques, respectively, in terms of Fractional Mean Reduction (FMR), Fractional Variance Reduction (FVR), Mean Field Bias (MFB) and Fractional Standard Error (FSE) of rainrate radar estimates with respect to raingauge data.

The $NN$ method denotes better scores than $ZR$ ones, especially when coupled to SNR for vertical profiles reconstruction (VPR by SNR). Results are generally much worse when there is no attempt to reconstruct (no VPR). Figure 6 shows the retrieved rainrate map by using NN method together with SNR approach for VPR reconstruction and histogram of accumulated rain measured by rain gauges during the whole event.

## 6 Conclusions

In this work it has been shown that in a complex orographic environment a hybrid technique, based on a combined statistical and a neural-network approach, can be successfully used to retrieve surface rainrate fields from partially-blocked C-band radar volume data.

Further work should be devoted to the analysis of a large set of rainfall case studies, possibly in various geographical mountainous regions.

*Acknowledgement.* This work has been partially supported by the Italian National Research Council (CNR) through GNDCI project and by Italian Ministry of Education, University and Research (MIUR).

## References

Andrieu, H., and Creutin, J.D. "Identification of vertical profiles of radar reflectivity for hydrological applications using an inverse method. Part I: Formulation", J. Appl. Meteor., 34, 225-239, 1995.

Aydin, K., Zhao, Y. and Seliga, T.A. "Rain-induced attenuation effects on C-band dual-polarization meteorological radars", IEEE Trans. Geosci. Remote Sens., 27, 57-66, 1989.

Borga, M., Anagnostou, E.N. and Frank, E. "On the use of real-time radar rainfall estimates for flood prediction in mountainous basins", J. Geophys. Res., 105-D2, 2269-2280, 2000.

Ciach, G.J. and Krajewski, W.F. "Radar-rain gauge comparisons under observational uncertainties", J. Appl. Meteor., 38, 1519-1525, 1999.

Cressman, G.P. "An operational objective analysis system", Mon. Wea. Rev., vol. 87, 367-374, 1959.

Delrieu, G., Andrieu, H. and Creutin, J. D. "Quantification of Path-Integrated Attenuation for X- and C-Band Weather Radar Systems Operating in Mediterranean Heavy Rainfall", J. Appl. Meteor., 39, 840-850, 2000.

French, M.N., Krawjeski, W.F. and Cuykendall, R. "Rainfall forecasting in space and time using a neural network", J. Hydrol., 137, 1-31, 1992.

Gray, W. R., Uddstrom, M. J. and Larsen, H. R. "Radar surface rainfall estimates using a typical shape function approach to correct for the variations in the vertical profile of reflectivity", Int. J. Rem. Sens., 23, 2489-2504, 2002.

Joss, J. and Lee, R. "The application of radar-gauge comparisons to operational precipitation profile corrections", J. Appl. Meteor., 34, 2612-2630, 1995.

Marzano, F.S., Mugnai, A., Smith, E.A, Xiang, X., Turk, J. and Vivekanandan, J. "Active and passive remote sensing of precipitating storms during CaPE. Part II: Intercomparison of precipitation retrievals from AMPR radiometer and CP-2 radar", Meteor. Atmospheric Physics, 54, 29-51, 1994.

Sauvageot, H. Radar meteorology, Artech House, Boston (MA), 1992.

Steiner, M, Houze, R.A. and Yuter, S.E. "Climatological Characterization of Three-Dimensional Storm Structure from Operational Radar and Rain Gauge Data", J. Appl. Meteor., 34, 1978-2007, 1995.

Vignal, B., Galli, G., Joss, J. and Germann, U. "Three methods to determine profiles of reflectivity from volumetric data to correct precipitation estimates", J. Appl. Meteor., 39, 1715-1726, 2000.